ROBOMECH Journal

RESEARCH ARTICLE

Open Access

Switching control of latex balloon expansion by using switching valve mediated with the Coanda effect

Kaneko Keita[1] and Takemura Kenjiro[2*]

Abstract

Soft robots have advantages in terms of safety, softness, and compliance compared to traditional robotic systems. However, fluid-driven soft actuators, often employed in soft robots, require a corresponding number of bulky pressure supplies/valves to drive. Here, we consider a valve that can control the flow without mechanical moving parts for simplifying the driving system of soft actuators. We developed a system comprising a pump, a switching valve, and two latex balloons to demonstrate the feasibility of introducing a fluid valve into soft robotics. As the valve, which makes use of the Coanda effect, can switch the flow between two outlets when the pressure difference between the outlets is 3 kPa, we employed a latex balloon connected to each outlet. The system can control the expansion of each balloon by switching the flow from the pump. The experimental results proved that the system could actuate each balloon.

Keywords: Soft robot, Fluidics, Coanda effect

Introduction

In recent years, there has been a growing demand for robots that can operate in human environments and be used for nursing, entertainment, customer service, etc. [1]. Such robots are expected to be safe to reduce possible physical harm when they come in contact with humans, flexible enough to behave similar to living organisms, and compliant enough to cope with unexpected situations and environments [2–4]. For these reasons, soft robots, in which the structure and actuators are flexible, have attracted wide attention [5].

Soft robots are often constructed and actuated using fluid-driven flexible rubber actuators [6]. Thus, a critical issue arises. When developing a soft robot, the mass and volume of the entire system increases as multiple pressure sources/valves are required based on the number of degrees of freedom of motion required by the robot. Therefore, a large number of studies have been reported on the application of pneumatic soft robots, where multiple motions were generated using a single compressor and several valves, suggesting the possibility of increasing the degrees of freedom with mechanically driven pneumatic components located outside a robot [7–9]. Considering that most multi-degree-of-freedom soft robots produce periodic motion, we do not necessarily control every actuator independently. They can be driven sequentially [7–9]. Compared to pneumatically driven soft robots, hydraulic systems for soft robotics have not yet been extensively explored. Previously reported hydraulic soft robots employ rigid and bulky fluid control components [10, 11].

Considering the abovementioned background, we focused on using a valve, as one of the most important elements of *fluidics*, to simplify the entire system. The idea is to realize a multi-degree-of-freedom motion by appropriately switching the pressure flow, generated by a pressure source, using a simple switching valve called

*Correspondence: takemura@keio.mech.ac.jp

[2] Department of Mechanical Engineering, Keio University, 3-14-1 Hiyoshi Kohoku-ku, Yokohama, Kanagawa 223-8522, Japan
Full list of author information is available at the end of the article

Bi-Stable Diverter [12]. In addition, there has been reported a quite smart idea of introducing a discharge flow of Bi-Stable Diverter into a control flow [13, 14]. By using the discharge flow as a feedback flow, a periodic motion of soft robots can be simply realized with one single pressure source and a Bi-Stable Diverter. To demonstrate this concept, the current study aims to realize a fluid-driven system that can selectively expand balloons using a Bi-Stable Diverter.

Materials and methods

Concept

Figure 1 shows a schematic of the proposed drive system, capable of selectively expanding each of the two balloons. The proposed drive system comprises a pump (not shown in the figure), a Bi-Stable Diverter, balloons, and throttle valves. The Bi-Stable Diverter switches the direction of the main flow, discharged from the pump into one outlet, using the Coanda effect [15] induced by the control flow. The throttle valve increases the gauge pressure of the balloon connected to the outlets; therefore, the gauge pressure of the target outlet of the switching valve is higher than that of the other. The difference in gauge pressure, due to the difference in flow rate, creates a difference in the balloon deformation. Switching the control flow causes the target outlet to switch, deflates the inflated balloon, and inflates the non-inflated balloon. This achieves a selective drive of multiple balloons with relatively simple configurations, thus, downsizing the entire system. It can be observed that there is a need for an additional control system for appropriately generating control flows 1 and 2. The control system may be implemented in a fluid circuit, for example, by feeding the outlet flow from the throttle valves to the control flow inlets to achieve a replicating motion of balloons. Therefore, this study simply shows that the Coanda effect employed in a simple fluidic valve may contribute to the selective drive of each balloon.

Bi-Stable Diverter

Figure 2a and b show an overview of the Bi-Stable Diverter, which is an important element in *fluidics*.

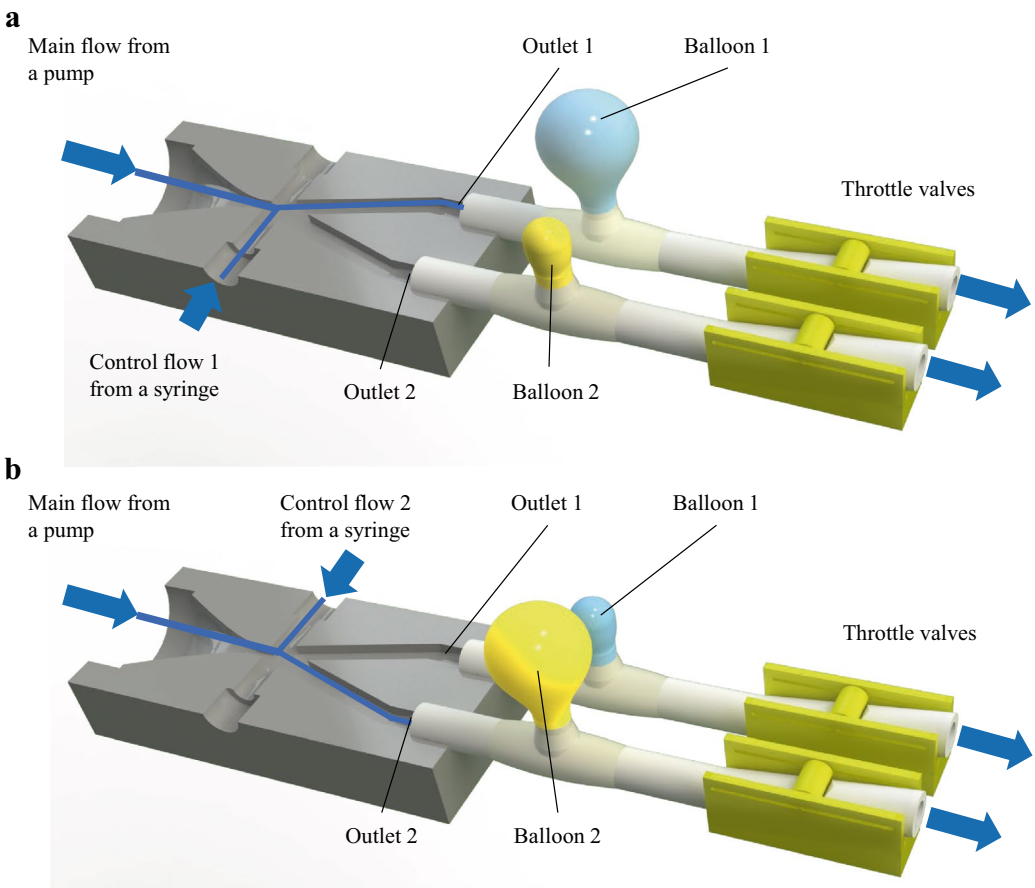

Fig. 1 Overviews of the proposed system to selectively drive balloons with simple fluidics valve mediated with the Coanda effect. **a** When the control flow 1 is introduced, **b** when the control flow 2 is introduced

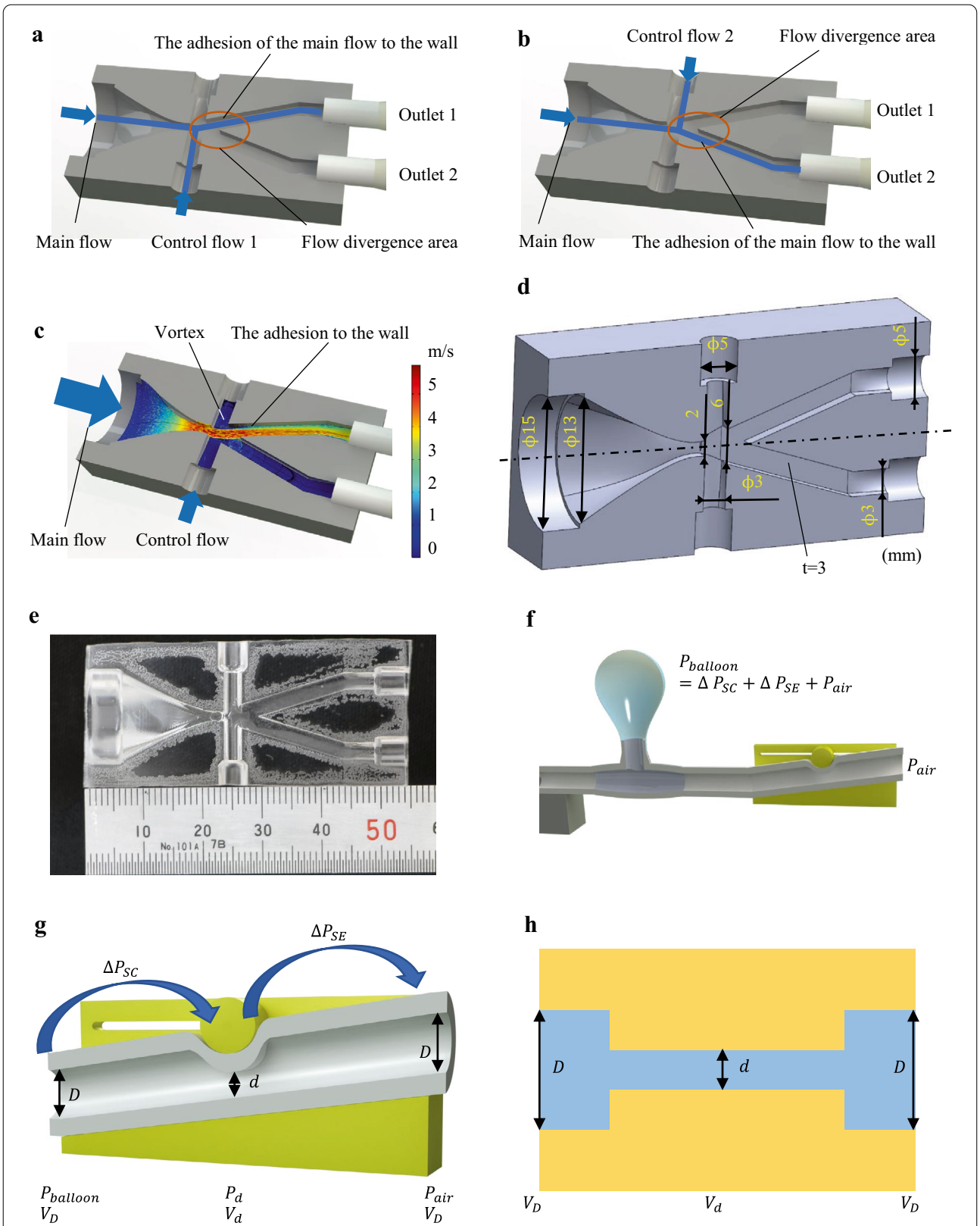

Fig. 2 Overviews of the fluidic switching valve and a throttle valve. **a** When the control flow 1 is introduced. **b** When the control flow 2 is introduced. **c** The Coanda effect observed in the fluidic switching valve. **d** Crosssection and dimensions of the developed fluidic switching valve. **e** Actual view of the valve. **f** An overview of the throttle valve. **g** Cross-section of the throttle valve. **h** A model of the throttle valve

Fluidics aims to realize logic circuits, such as electronic circuits, using fluid flow. To achieve this, many fluidic logic elements employ the Coanda effect, in which fluid flow along a channel adheres to a channel wall [16]. We used this digital switching function for driving soft actuators. A Bi-Stable Diverter can select the discharge outlet of the flow from the pump (main flow) by inputting a small amount of flow from the side (control flow). In other words, the main flow can be directed into outlet 1 by inputting control flow 1, and the same is true for outlet 2 (see Fig. 2).

Figure 2c shows a schematic of the Coanda effect observed in the Bi-Stable Diverter. The flow velocity distribution is mapped on the model, which was calculated using the k-ε turbulence model for a low Reynolds number. Note that the condition for the numerical simulation is as follows: the main flow velocity is 0.7 m/s; the control flow 1 velocity is 0.04 m/s; the control flow 2 velocity is 0 m/s. As shown in Fig. 2a, b, and c, the difference in the discharge flow rate between the outlets was created by the negative pressure in a vortex created by the Coanda effect at the flow divergence area. The Coanda effect refers to the fluid property in which the jet flows along a curved surface and is less prone to flow separation than a uniform flow [17]. For this reason, in the Bi-Stable Diverter, shown in Fig. 2c, the main flow adheres to the wall on either side of the direction of the flow in the separation area. The valve can select the wall that the main flow should adhere to by introducing a control flow perpendicular to the main flow at the flow divergence area, which means that the valve can switch the discharge outlet.

Figure 2d and e show the dimensions and an actual view of the developed Bi-Stable Diverter, whose dimension is based on that in ref. 17. The diameters of the main flow inlet, control flow inlet, and outlet were 13 mm, 3 mm, and 3 mm, respectively. The cross-section of an orifice, where the main flow and control flow collide, was a rectangle with a width of 2 mm and a thickness of 3 mm. Water was employed as the working fluid.

Throttle valve

Figure 2f, g, and h show schematics of the throttle valve and its model. The throttle valve intentionally creates pressure loss according to the flow rate through the valve. The pressure loss, ΔP, can be calculated using the loss coefficients, K, as

$$\Delta P = K\frac{\rho V^2}{2}, \tag{1}$$

where ρ is the density, and V is the velocity. Therefore, the pressure loss is proportional to the square of the velocity. In addition, the loss function K can be considered as that for sudden contraction, K_{SC}, and that for sudden expansion, K_{SE}. The theoretical loss coefficient for a sudden expansion is expressed as

$$K_{SE} = \left(1 - \frac{d^2}{D^2}\right)^2, \tag{2}$$

where d is the diameter of the narrow area of the tube, and D is the diameter of the wide area of the tube. In addition, the loss coefficient for a sudden contraction fits the empirical formula as

$$K_{SC} \approx 0.42\left(1 - \frac{d^2}{D^2}\right) \tag{3}$$

up to the value $d/D = 0.76$, above which it merges into Eq. (2). Therefore, the total pressure loss, which equals the inner pressure of the balloon, can be written as:

$$\begin{aligned} c\Delta P_{total} &= K_{SC}\frac{\rho {V_D}^2}{2} + K_{SE}\frac{\rho {V_d}^2}{2} \\ &= \frac{\rho {V_D}^2}{2}\left[0.42\left(1 - \frac{d^2}{D^2}\right) + \frac{D^2}{d^2}\left(1 - \frac{d^2}{D^2}\right)^2\right] \end{aligned} \tag{4}$$

$$\because V_d\frac{1}{4}\pi d^2 = V_D\frac{1}{4}\pi D^2.$$

Note that these equations can be applied only to sudden extraction (contraction). However, we employed a roller clamp (KT-6, Cole-Parmer LLC, USA) as the throttle valve, to obtain well-rounded entrance and exit of the throttle valve. Therefore, the actual loss coefficient for contraction is considered negligible ($K = 0.05$), and that for extraction is considered to be lower than that for sudden expansion [18].

Balloon

As shown in Fig. 2a and b, directing the main flow to outlet 1 (2) creates a difference in the discharge flow rate between the outlets. This flow rate difference causes the gauge pressure of the balloon to be connected to the outlets owing to the throttle valve (cf. Figs. 1 and 2c). Therefore, the differential deformation in the balloon is achieved by the pressure difference, ΔP, which depends on the flow rate difference between the outlets of the fluidic valve. However, as shown in Fig. 2c, the flow rate difference produced by the Bi-Stable Diverter depends on the Coanda effect at the flow divergence area. Therefore, the Bi-Stable Diverter cannot maintain the flow rate difference if the pressure applied to the target outlet is large.

To ensure sufficient deformation difference between the balloons, we employed a latex balloon. Figure 3a and b show schematic PV diagrams of a balloon with (a) linear and (b) nonlinear relation between the internal pressure and volume. In the case of a balloon with a linear

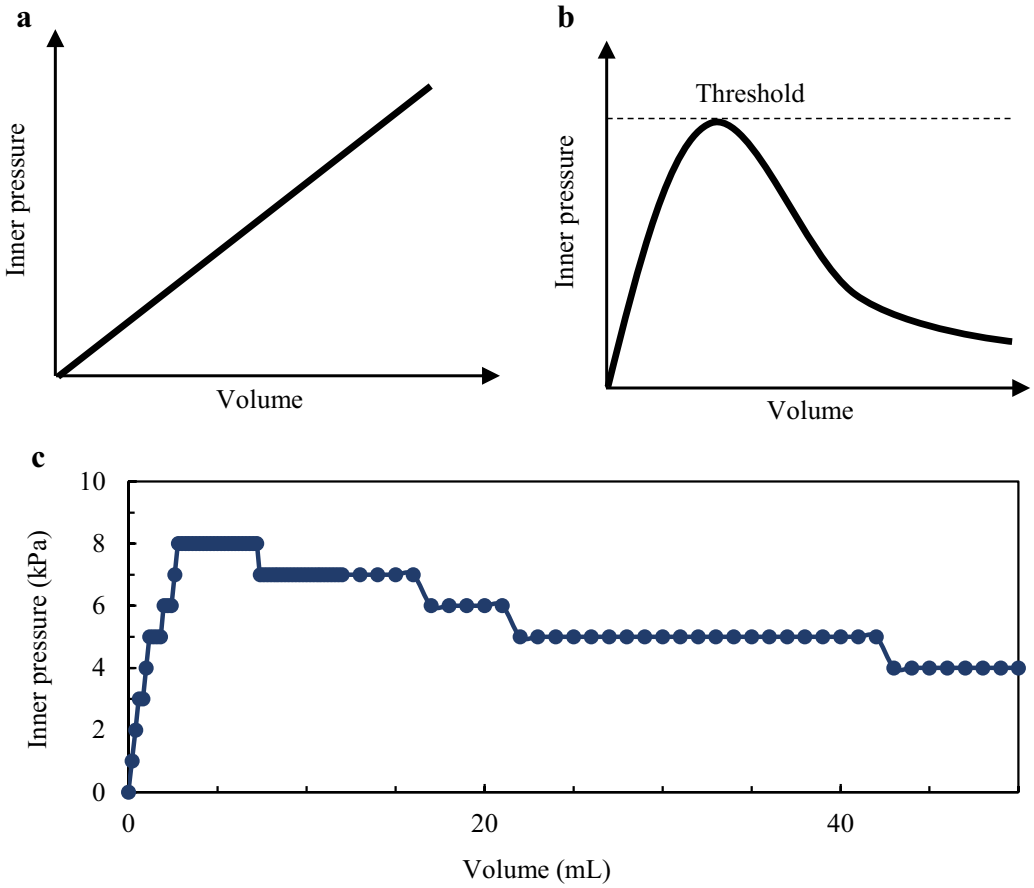

Fig. 3 PV diagrams of a balloon. **a** Linear PV diagram. **b** Nonlinear PV diagram with a peak. **c** PV diagrams of a latex balloon employed in this study

PV diagram (a), ΔP must be large to produce a sufficient deformation difference. On the other hand, a balloon with a peak in the PV diagram (b) deforms slightly up to a threshold pressure and deforms significantly at the threshold pressure and beyond. In other words, it is possible to produce a sufficient deformation difference between the balloons with a peak in their PV diagram when the gauge pressure difference, ΔP, exceeds the threshold value.

Figure 3c shows the PV diagram of the latex balloon employed in this study. The PV diagram was measured by injecting water into the balloon with syringes (SS-50ESZ and SS-10ESZ, Terumo Corporation, Japan). The balloon was injected with water in a 0.2 mL step up to 12 mL and later, in a 1 mL step. The internal pressure of the balloon was measured with a pressure gauge (GC-31–174, Nagano Keiki Co., Ltd., Japan) at each step. The peak internal pressure on the PV diagram was 8 kPa when the volume of the balloon was approximately 5 mL. Beyond this, the internal pressure decreased as the volume increased. It was confirmed that the balloon deformed significantly at a threshold value of approximately 8 kPa and higher.

Fabrication of components

Figure 4 shows the developed system. The system consisted of a positive displacement pump (V-15, Iwaki Corporation, Japan), a Bi-Stable Diverter developed in this study, syringes (SS-50ESZ, Terumo Corporation, Japan), tubing connectors (TPX Tubing Connector 3549, Sanwaplatec Co., Ltd., Japan), balloons (polka dot balloon, Tiger Rubber Co., Ltd., Japan), and throttle valves. The balloons were connected to the Bi-Stable Diverter via tubing connector. Water was as the working fluid in the subsequent experiments.

Experimental results and discussion

Switching characteristics

Figure 5a shows the experimental setup for switching characterization. The positive displacement pump was connected to the main flow inlet of the Bi-Stable Diverter, and

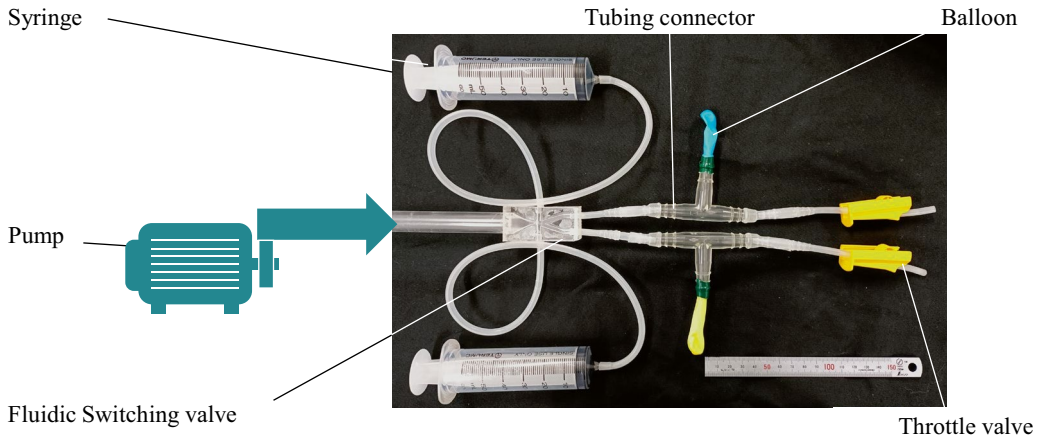

Fig. 4 An actual view of the developed system to confirm the feasibility of introducing the fluidic switching valve to soft actuator system.

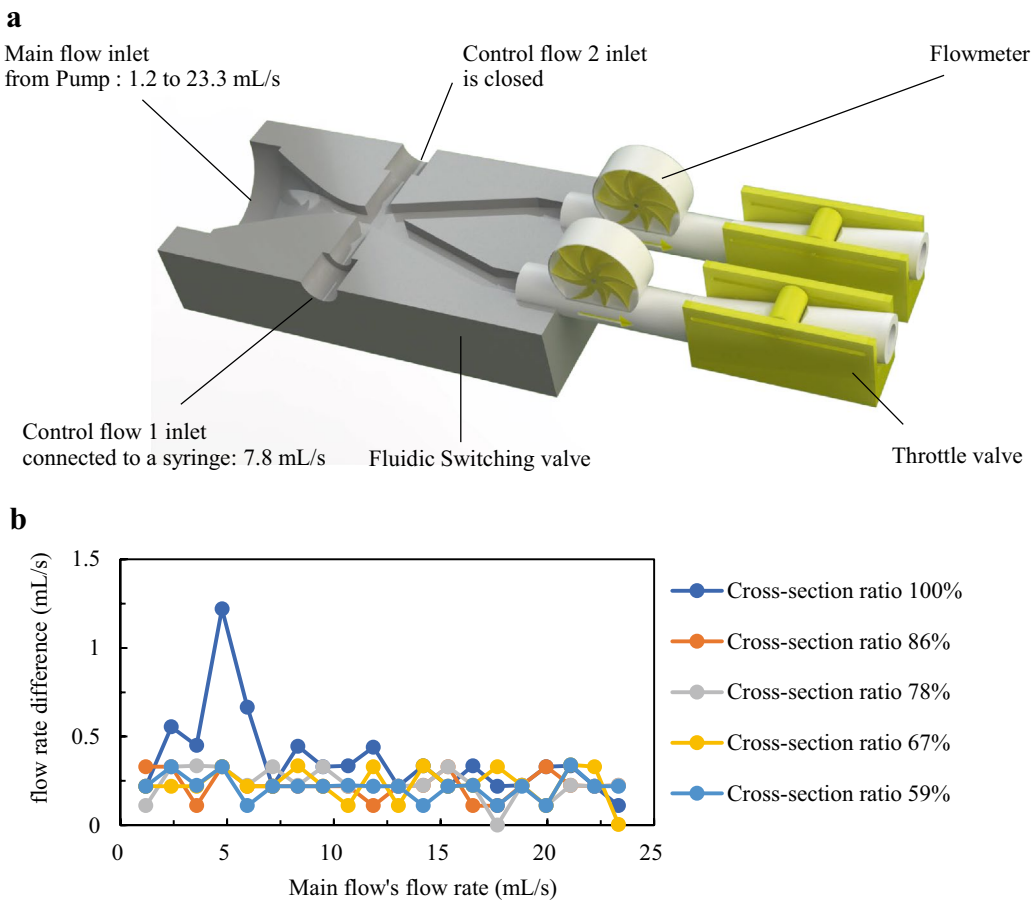

Fig. 5 The experiment for switching characterization. **a** The set up for the experiment. **b** the flow rate difference of the outlet 1 against outlet 2

the control flow inlet 2 was closed. The syringe was connected to control flow inlet 1 to direct the main flow to outlet channel 1. A flowmeter (SEN-HZ06K, Uxcell, China) was connected to each outlet to measure the flow rate along each outlet channel. The flow rate of the main flow was varied from 1.2 to 23.3 mL/s in 20 equal intervals, and

the flow rate of control flow 1 was set to 7.8 mL/s. In addition, the cross-section ratio of the throttle valve, connected to each outlet, was varied from 59 to 100% (fully closed) in five intervals. Figure 5b shows the flow rate difference between the outlet 1 and outlet 2 ($Q_{out\,1} - Q_{out\,2}$). The volumetric flow rate discharged from the outlet 1 was about 0.25 mL/s higher than that from the outlet 2 in almost all conditions.

Balloons deformation

The deformation of the balloon was visually recorded with different combinations of parameters, main flow rate and cross-section ratio of the throttle valve. The flow rate of main flow was varied from 1.2 to 23.3 mL/s in 20 equal intervals. In addition, the cross-section ratio of the throttle valve ranged from 59 to 100% in 5 intervals. The flow rate of the control flow 1 was set to 7.8 mL/s, and the control flow 2 was closed. The main flow and control flow 1 were introduced at t = 0 s, and after a sufficient time (7.6 s, time at which the syringe was empty), the flow stopped.

Figure 6a and b show the defined status of the balloons and a summary of the experimental results. We defined the behavior of the balloon as follows: (a) both balloons are always inflated with or without control flow, (b) one of the balloons inflates but does not deflate when the control flow is stopped; (c) one of the balloon inflates at will and deflates when the control flow is stopped (desired behavior), (d) one or both balloons do not inflate much, and (e) neither of the balloons inflate at all. Figure 6c shows the deformation of the balloons at a cross-section ratio of 59% and a flow rate of 9.5 mL/s for the main flow. The time required for the blue balloon to deflect under this condition was 4 s and that for the yellow balloon was 6 s. Figure 6d shows the deformation of the balloon at a cross-section ratio of 59% and a flow rate 10.8 mL/s for the main flow. Under this condition, the time required for the blue balloon to deflect was 12 s and that for the yellow balloon was 83 s. (i) and (iv) in Fig. 6c and d show the initial state of the balloons at t or $t' = 0$ s. Note that t and t' represent the time for introducing the control flows 1 and 2, respectively. When the water in the syringe is fully injected at t (t') = 7.6 s, the balloons appear as shown in (ii) and (v). After sufficient time for deflection, the balloons restore their initial shape, as shown in (iii) and (vi). The time required for the balloons to fully deflect depends on the experimental conditions. Note that (i–iii) are for the blue balloon to be expanded, and (iv–vi) are for the yellow balloon. These experimental results indicate that balloons can be selectively driven by setting appropriate inflow conditions.

Discussion

Here, we discuss why the desired deformation (defined as (c) in Fig. 6a) is distributed diagonally in Fig. 6b, and why there is a difference in time required to restore the initial appearance among the different conditions as shown in Fig. 6c and 6d.

Figure 7 shows a schematic relation between the flow rate of the main flow, Q, and the cross-section ratio of the throttle valve, γ. If the Q increases slightly as

$$Q' = Q + \Delta Q, \tag{5}$$

The flow rates of outlets 1 and 2 increase (see Fig. 5). The inner pressure of the balloon increases as a function of the throttle valve, and it is proportional to the outlet flow velocity (see Eq. 4). Therefore, if the flow rate of the main flow becomes Q', the inner pressure of both balloons increases, and vice versa. If γ decreases slightly as

$$\gamma' = \gamma - \Delta\gamma, \tag{6}$$

The inner pressure of both balloons increases, and vice versa. Therefore, if the balloons deform suitably, as shown in Fig. 6a (c) at the point (Q, γ) in Fig. 7, the close suitable point may be located at $(Q + \Delta Q, \gamma + \Delta\gamma)$ and $(Q - \Delta Q, \gamma - \Delta\gamma)$. Then, the relationship between ΔQ and $\Delta\gamma$ should be clarified to understand the reason for the diagonally located experimental result of the desired deformation in Fig. 6b. As we neglect the pressure loss from sudden contraction in Eq. 4, the inner pressure of the balloon is expressed as

$$\Delta P_{total} = \frac{\rho V_D^2}{2} \frac{D^2}{d^2} \left(1 - \frac{d^2}{D^2}\right)^2. \tag{4'}$$

As shown in Eq. 4′, the pressure is expressed as the product of the square of the flow velocity, V_D, and the fourth power of the inner diameter ratio at the throttle valve. However, as we use the roller clamp as the throttle valve, Eq. 4′ can be expressed, using the cross-section ratio γ of the tube instead of the inner diameter ratio, as

$$\Delta P_{total} = \frac{\rho V_D^2}{2} \frac{1}{\gamma} (1 - \gamma)^2 = \frac{\rho V_D^2}{2} \left(\frac{1}{\gamma} + \gamma - 2\right). \tag{4''}$$

(See figure on next page.)

Fig. 6 Balloons deformation experiment. **a** An evaluation status defined in this experiment. **b** The summary of the experimental results. **c** The balloon's deformation under the cross area of 59%, the flow rate of main flow of 9.5 mL/s. (i) t = 0 s: inflow started. (ii) t = 7.6 s: the control flow 1 was stopped. (iii) t = 12 s: the balloon contracted. (iv) t′ = 0 s: inflow started. (v) t′ = 7.6 s: the control flow 2 was stopped. (vi) t′ = 14 s: the balloon contracted. **d**) The balloon's deformation under the cross area of 59%, the flow rate of main flow of 10.8 mL/s. (i) t = 0 s: inflow started. (ii) t = 7.6 s: the control flow 1 was stopped. (iii) t = 20 s: the balloon contracted. (iv) t′ = 0 s: inflow started. (v) t′ = 7.6 s: the control flow 2 was stopped. (vi) t′ = 83 s: the balloon contracted

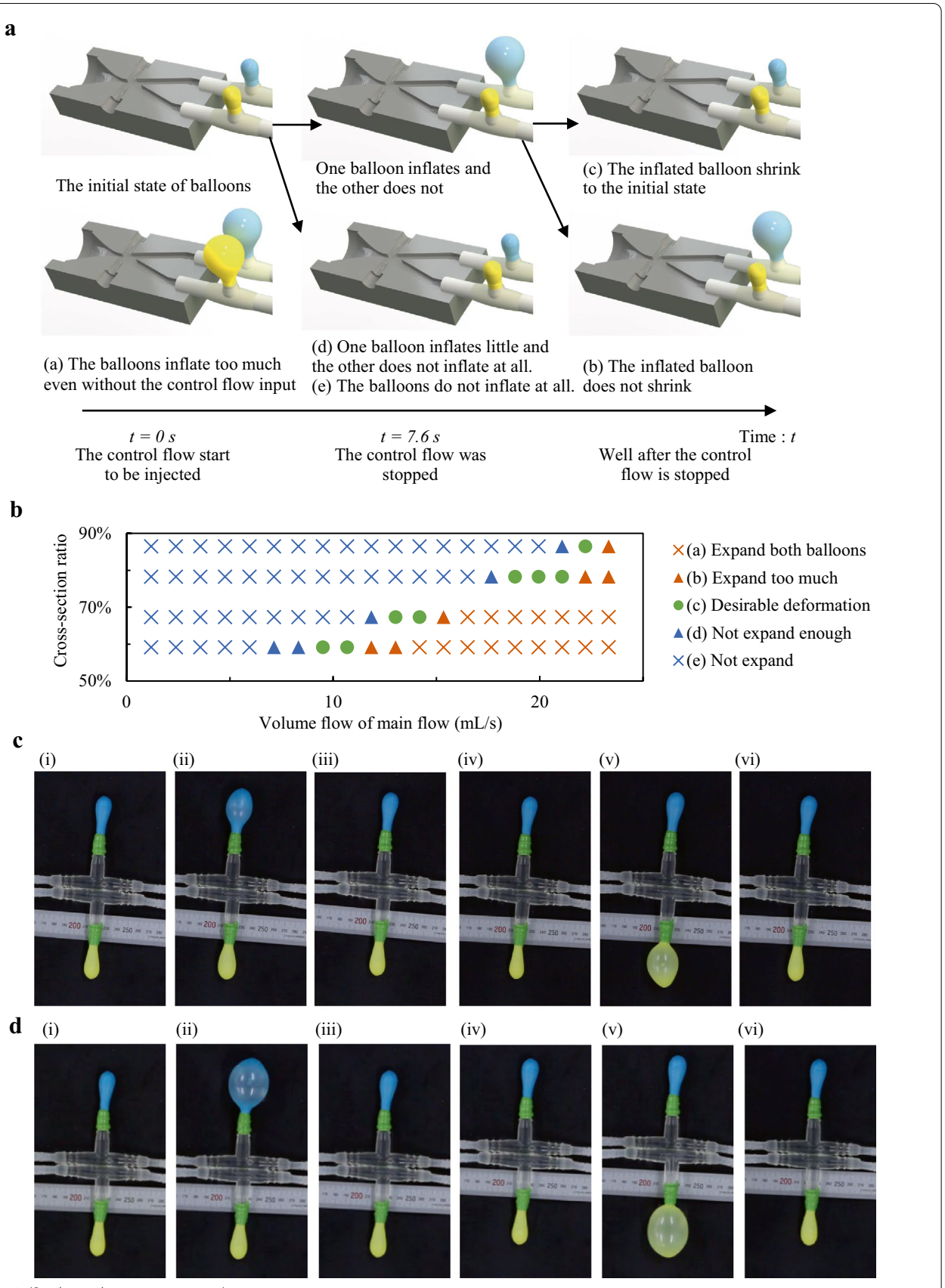

Fig. 6 (See legend on previous page.)

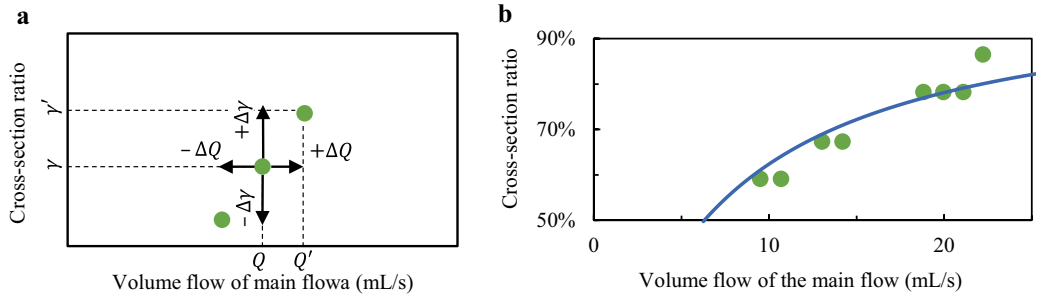

Fig. 7 The relation between the main flow rate and the cross-section ratio. **a** Schematic relation. **b** Comparison between the experimental result and the solution of the pressure loss

We solved Eq. 4″ for $Q(= V_d A)$,γ, and the constant left-hand side, $\Delta P_{total} = 8$ kPa, at which the PV diagram shows a peak (see Fig. 3c). Note that the cross-section, A, was set for $\Delta P_{total} = 8$ kPa when $Q = 13$ mL/s and $\gamma = 0.67$. We superimposed the solved relation between Q and γ onto the desired conditions to obtain the appropriate deformation of balloons (c) in Fig. 6a) in Fig. 7b. Even though there is a slight difference, Eq. 4″ predicts the diagonal tendency in the graph. When the cross-section ratio is greater than 80%, Eq. 4″ underestimates the cross-section ratio. The reason may be a pressure loss due to the viscosity and bending of the tube in the actual experimental system. As a result, in an actual situation, the pressure loss increases as the flow rate of the main flow increases, resulting in a lower suitable flow rate. Since the balloons require a threshold pressure of 8 kPa to significantly deform, the inlet flow rate should be sufficiently high or the cross-section ratio should be small enough to obtain this threshold pressure. In other words, when the combination of the flow rate of the main flow and cross-section ratio is not suitable, the inner pressure of the balloon is not high enough to sufficiently inflate the balloon. Therefore, the plots of the desired deformation are located diagonally, as shown in Fig. 6b.

When the flow rate of the main flow was high and the balloon inflated ((i) to (ii), and (iv) to (v) in Fig. 6c and d), the inner pressure of the balloon increased and then decreased by ΔP_{def} according to the deformation of the balloon, owing to the nonlinear PV diagram shown in Fig. 3c. This means that once the inner pressure exceeds the threshold, it becomes easier for the inflated balloon to inflate, and the deflated balloon to deflate. Therefore, the smaller the ΔP_{def} is, the easier it is for the balloon to deflate ((ii) to (iii), and (v) to (vi) in Figs. 6c and d) after the control flow is stopped. The deformability of the balloon depends on ΔP_{def}, which depends on the deformation of the balloon when the control flow is stopped. Moreover, the deformation of the balloon depends on the flow rate of the main flow. Therefore, the time required for the deflation of the balloon increases as the flow rate of the main flow increases. Note that in Fig. 6d, the 10.8 mL/s of flow rate of the main flow requires a longer time for deflection compared with Fig. 6c, in which the flow rate of the main flow is 9.5 mL/s.

Finally, the effectiveness of the feedback loop for periodically driving a soft robot is discussed. In this study, the control flow was fixed at 7.8 mL/s in the experiments. Therefore, if a feedback flow is provided, the feedback flow should be greater than 7.8 L/min. As shown in Fig. 6b, more than 50% of the total inflow was discharged from the outlet on the actuated side under all experimental conditions. Therefore, it can be assumed that the feedback flow is equivalent to or greater than the control flow employed in this study when the flow rate of main flow is 15.6 mL/s or higher.

Conclusion

To realize the multi-degree-of-freedom motion of a soft robot using embedded fluidic elements, this study proposed a method to selectively inflate a balloon using a fluidic valve, mediated by the Coanda effect, operated by the control flow input. The developed valve is capable of generating a flow difference of approximately 0.25 mL/s between two outlets, and the selective inflation of balloons is realized using a simple configuration when the balloons have peaks in their PV diagram. This shows the possibility of a new driving method for fluid-driven soft robots and that a soft robot with multiple degrees of freedom can be driven only by fluid elements. Because the proposed method suggests that the control strategy may be implemented in the fluid circuit, our future study will focus on the development of a fully fluidically controlled soft robot system.

Acknowledgements
We would like to thank Editage (www.editage.com) for English language editing.

Author contributions
KT conceived and designed the experiments; KK developed the experimental system, performed the experiments, and analyzed the data. KK wrote the paper with critical input from KT. Both the authors read and approved the final manuscript.

Funding
Not applicable.

Availability of data and materials
The datasets used and/or analyzed in this manuscript are available from the corresponding author upon reasonable request.

Declarations

Competing interests
The authors declare that they have no competing interests.

Author details
[1]Graduate School of Science and Technology, Keio University, 3-14-1 Hiyoshi Kohoku-ku, Yokohama, Kanagawa 223-8522, Japan. [2]Department of Mechanical Engineering, Keio University, 3-14-1 Hiyoshi Kohoku-ku, Yokohama, Kanagawa 223-8522, Japan.

Received: 24 December 2021 Accepted: 8 May 2022
Published online: 26 May 2022

References

1. Nishioka Y (2015) Pneumatic soft robot arm. J Robot Soc Jpn 33(9):664–667. https://doi.org/10.7210/jrsj.33.664
2. Kim S, Laschi C, Trimmer B (2013) Soft robotics: a bioinspired evolution in robotics. Trends Biotechnol 31(5):287–294. https://doi.org/10.1016/j.tibtech.2013.03.002
3. Shepherd RF, Ilievski F, Choi W, Morin SA, Stokes AA, Mazzeo AD, Chen X, Wang M, Whitesides GM (2011) Multigait soft robot. Proc Natl Acad Sci USA 108(51):20400–20403. https://doi.org/10.1073/pnas.1116564108
4. Katzschmann RK, DelPreto J, MacCurdy R, Rus D (2018) Exploration of underwater life with an acoustically controlled soft robotic fish. Sci Robot. https://doi.org/10.1126/scirobotics.aar3449
5. Takemura K (2018) Soft robotics using electro-conjugate fluid (in Japanese). Meas Control 57(11):775–779
6. Cacucciolo V, Shintake J, Kuwajima Y, Maeda S, Floreano D, Shea H (2019) Stretchable pumps for soft machines. Nature 572(7770):516–519. https://doi.org/10.1038/s41586-019-1479-6
7. Gorissen B, Milana E, Baeyens A, Broeders E, Christiaens J, Collin K, Reynaerts D, De Volder M (2019) Hardware sequencing of inflatable nonlinear actuators for autonomous soft robots. Adv Mater 31(3):e1804598. https://doi.org/10.1002/adma.201804598
8. Zatopa A, Walker S, Menguc Y (2018) Fully soft 3D-printed electroactive fluidic valve for soft hydraulic robots. Soft Robot 5(3):258–271. https://doi.org/10.1089/soro.2017.0019
9. Wehner M, Truby RL, Fitzgerald DJ, Mosadegh B, Whitesides GM, Lewis JA, Wood RJ (2016) An integrated design and fabrication strategy for entirely soft, autonomous robots. Nature 536(7617):451–455. https://doi.org/10.1038/nature19100
10. Galloway KC, Becker KP, Phillips B, Kirby J, Licht S, Tchernov D, Wood RJ, Gruber DF (2016) Soft robotic grippers for biological sampling on deep reefs. Soft Robot 3(1):23–33. https://doi.org/10.1089/soro.2015.0019
11. Polygerinos P, Wang Z, Galloway KC, Wood RJ, Walsh CJ (2015) Soft robotic glove for combined assistance and at-home rehabilitation. Robot Auton Syst 73:135–143. https://doi.org/10.1016/j.robot.2014.08.014
12. Tesař V, Bandalusena HCH (2011) Bistable diverter valve in microfluidics. Exp Fluids 50(5):1225–1223. https://doi.org/10.1007/s00348-010-0983-0
13. Sieber M, Ostermann F, Woszidlo M, Oberleithner K, Paschereit C (2016) Lagrangian coherent structures in the flow field of a fluidic oscillator. Phys Rev Fluids. https://doi.org/10.1103/PhysRevFluids.1.050509
14. Tesař V (2016) Taxonomic trees of fluidic oscillators. In: Dančová P (ed) EFM16—experimental fluid mechanics. EDP Sciences, Mariánské Lázně. https://doi.org/10.1051/epjconf/201714302128
15. Tesař V (2004) Fluidic valve for reactor regeneration flow switching. Chem Eng Res Des 82(3):398–408. https://doi.org/10.1205/026387604322870516
16. Bettridge M, Smith B, Spal R (2004) Aerodynamic jet vectoring using steady blowing and suction. Exp Fluids 40:776–785
17. Furuta R, Takeuti R, Itagaki H, Okumura T (1983) Studies on the fluid control III—fundamental study on the discharge control by fluidics. Res Bull Fac Coll Agric Gifu Univ 48:147–157
18. White MF (ed) (2016) Fluid mechanics. McGraw-Hill Education, New York

Publisher's Note